

# Effect of particle trapping on frost heaving soils

(Stephen S. L. Peppin, Victoria, Canada)  
*email:* speppin@gmail.com

## Abstract

A model of freezing soils is developed that accounts for the dependence of the frost heave rate on particle trapping. At sufficiently low cooling rates the soil experiences primary frost heave with a single growing ice lens that rejects all soil particles. At higher cooling rates ice lenses start to engulf the largest soil particles and the rate of segregation heave is reduced. At the highest freezing rates all particles are engulfed by the ice and the pore water freezes *in situ*. A new kinetic expression for the segregation potential of the soil is obtained that accounts for particle trapping. Using this expression a simple transient frost heave model is developed and compared with experimental data.

## 1 Introduction

Frost heave is the uplift of the soil surface as it freezes, and generally involves two components: an *in situ* heave caused by the 9% density difference between water and ice, and a segregation heave caused by the formation of discrete ice lenses in the soil [1, 2]. While many aspects of frost heave have been explained in recent years, one intriguing phenomenon that has received less attention is the dependence of the rate of heave on the rate at which the soil is frozen. Beskow [3] showed that the heave rate is under certain conditions independent of the freezing rate; upon changing the surface temperature of a soil sample from  $-2^{\circ}\text{C}$  to  $-10^{\circ}\text{C}$ , it was observed that the rate of heaving remained constant [3, p.79]. He noted, however, that the independence held only as long as the freezing front was descending into the soil. Once the freezing front became stationary (relative to the laboratory frame), a single final ice lens formed and the rate of heave was proportional to the rate of freezing [3]. Horiguchi [4], Penner [5] and Konrad [6] observed similar results, while also showing that at very high rates of freezing the frost heave rate begins to decrease; at the highest freezing rates no segregation heave occurs at all, and the only heave is due to the volume expansion of the pore water as it freezes.

Related to these observations are the experiments of Corte [7–9]. He found that when freezing a soil with a particle size distribution, at very low freezing rates a single ice lens pushes ahead all particles (segregation freezing). At higher rates the ice lens begins to engulf the largest particles, while pushing the smaller particles ahead, leading to a sorting process at the ice lens surface. As the freezing rate increases further the ice lens engulfs ever smaller particles, until all particles are engulfed beyond a critical freezing rate (*in situ* freezing). Similar observations have been made by Jackson and Uhlmann [10], Branson [11] and Matsuoka *et al* [12].

Konrad and Morgenstern [13] found that at very low freezing rates in a transient frost heave experiment, near the time when the final ice lens forms, the rate of segregation heave is proportional to the temperature gradient at the ice lens. The constant of proportionality, which they called the segregation potential (SP), is a soil parameter independent of the freezing path. They defined the segregation potential as

$$SP = v_w/G_T, \quad (1)$$

where  $v_w$  is the measured water intake rate at the initiation of the final ice lens and  $G_T$  is the temperature gradient in the frozen fringe region. Here, as in Konrad and Morgenstern [13], the frozen fringe is defined as the region of soil between the warmest ice lens and the  $0^{\circ}\text{C}$  isotherm. This definition is convenient as it applies whether or not the frozen fringe contains pore ice [14, 15].

---

*For God so loved the world, that He gave His only begotten Son, that whosoever believeth in Him should not perish, but have everlasting life. For God sent not His Son into the world to condemn the world; but that the world through Him might be saved. John 3:16-17*

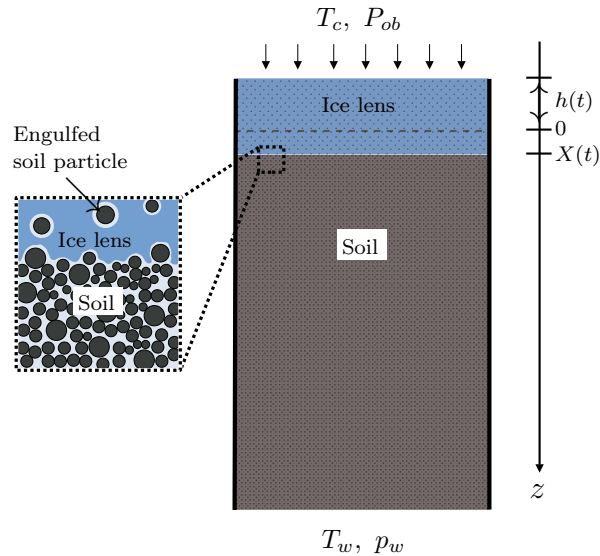


Figure 1: Schematic of a column of soil freezing from the top down, with an ice lens at the surface. Because of particle trapping the ice lens is not pure, but contains a volume fraction  $\phi_i$  of engulfed soil particles. The horizontal dashed line shows the original unheaved surface of the soil. The total amount of frost heave  $h(t)$  increases because of the expansion of water as it freezes and because of excess water drawn to the ice lens from the water table. As the ice lens engulfs particles, the freezing front  $X(t)$  moves downward into the soil.

Konrad and Morgenstern tabulated  $SP$  as a function of soil properties, overburden pressure and salinity for a variety of soils [16, 17], and several studies by them and others have demonstrated its usefulness in the prediction of frost heave rates in field situations [18–24]. However, a shortcoming of frost heave models based on the  $SP$  concept is a tendency to overpredict the rate of frost heave at early times in step freezing tests, when the freezing rate is high [16, 19, 20, 25, 26]. As noted by Konrad and Morgenstern [6, 27], Sego *et al.* [25] and Svec [26], at very high freezing rates  $SP$  is no longer a unique function of soil properties but depends also on the rate of freezing. This is in part because at very high freezing rates the soil water freezes *in situ* and the water intake rate  $v_w$  approaches zero, or can even be negative (water expulsion) [17, 28].

Recently a theoretical expression for the segregation potential in saline soils has been obtained by considering the linear stability of an ice lens during primary frost heave [29]. Here a similar approach is taken that also accounts for the effects of particle trapping. This leads to a new *kinetic* expression for the segregation potential that depends on the rate of freezing. In Section 3 the basic equations describing conservation of mass and energy at an ice lens are described, and conditions for the onset of hydraulic supercooling obtained in the presence of particle trapping. In Section 4 a constitutive equation for the particle distribution coefficient at the ice lens surface is obtained and compared with experimental data. In Section 5 an expression for the kinetic segregation potential that accounts for particle trapping is obtained, and employed in Section 6 to predict the heave rate in a field frost heave experiment and above a buried natural gas pipeline.

## 2 Effect of particle trapping on frost heave

The system to be studied is illustrated in figure 1. There is a single stable ice lens growing within a water-saturated soil under an overburden pressure  $P_{ob}$ , with surface temperature  $T_c < 0^\circ\text{C}$ . At the base of the soil the temperature is held at  $T_w > 0^\circ\text{C}$  and the pore pressure is maintained at

atmospheric  $p_w$  via a fluid reservoir or water table. The total frost heave rate is

$$\dot{h} = \dot{h}_s + \dot{h}_i, \quad (2)$$

where  $\dot{h}_s$  is the segregation heave rate and  $\dot{h}_i$  is the *in situ* heave rate. Because the ice lens is engulfing soil particles, the freezing front  $X(t)$  is moving downward into the soil. The dashed line in figure 1 shows the original unheaved surface  $z = 0$  of the soil before freezing began. The upper heaved surface of the soil is increasing in height both because of the expansion of the pore water as it freezes ( $\dot{h}_i$ ) and because excess water is drawn to the freezing front from the reservoir ( $\dot{h}_s$ ).

In general obtaining expressions for  $\dot{h}_s$  and  $\dot{h}_i$  as functions of the freezing conditions is a challenging task. Here, following Konrad and Morgenstern [16] it is assumed that for field situations the segregation and *in situ* heave rates are given by the expressions

$$\dot{h}_s = \frac{\rho_w}{\rho_i} v_w \quad \text{and} \quad \dot{h}_i = \left( \frac{\rho_w}{\rho_i} - 1 \right) n \dot{X}, \quad (3)$$

where  $n$  is the porosity of the unfrozen soil,  $\dot{X} = dX/dt$  is the rate at which the freezing front moves into the soil, and  $\rho_w$  and  $\rho_i$  are the densities of water and ice [16, 18]. As noted by Nixon [30], the above equations do not account for the water expulsion ( $v_w < 0$ ) that occurs in some frost heave experiments at early times and high overburden pressures [31, 32]. However, the effect is not typically important in field frost heave situations [16, 28] and is neglected here for simplicity.

Because of particle trapping the ice lens is not pure, but contains a volume fraction  $\phi_i$  of soil particles equal to

$$\phi_i = k_p \phi, \quad (4)$$

where  $\phi = 1 - n$  is the soil particle volume fraction in the unfrozen soil and  $k_p$  is the particle distribution coefficient at the ice lens surface, described in more detail below. When  $k_p = 0$ , the ice lens is pure and the freezing front is stationary ( $\dot{X} = 0$ ). When  $k_p = 1$ , the ice lens engulfs all particles and the soil freezes *in situ* with no ice segregation.

Neglecting the effect of the density difference between water and ice on the segregated ice growth rate, an expression for  $\dot{h}_s$  as a function of  $k_p$  can be obtained as follows. As the ice lens engulfs particles, the freezing front  $X(t)$  moves downward into the unfrozen soil at rate  $\dot{X}$ . The total freezing rate of the soil is

$$V = \dot{X} + \dot{h}_s. \quad (5)$$

Conservation of soil particle number at the freezing front (lower ice lens surface) can be written as

$$\phi_i V = \phi \dot{X}, \quad (6)$$

which ensures that the particle flux  $\phi_i V$  entering the ice lens is the same as the flux  $\phi \dot{X}$  leaving the soil. Combining (4)–(6) then gives

$$\dot{X} = k_p V \quad \text{and} \quad \dot{h}_s = (1 - k_p)V. \quad (7a,b)$$

With (7) the total heave rate  $\dot{h}$  can be written as

$$\dot{h} = \dot{h}_s + \dot{h}_i = (1 - k_p)V + \left( \frac{\rho_w}{\rho_i} - 1 \right) n k_p V. \quad (8)$$

At low freezing rates  $V \ll V_c$ , where  $V_c$  is the critical trapping speed of the soil particles [33, 34], the ice lens rejects all the particles and  $k_p = 0$ . In this primary frost heave case the ice lens is pure, the freezing front is stationary ( $\dot{X} = 0$ ) and the rate of frost heave is  $\dot{h} = \dot{h}_s = V$ . At very high freezing rates  $V \gg V_c$ , the ice engulfs all of the particles ( $k_p = 1$ ) and the pore water freezes *in situ* with  $\dot{h}_s = 0$ . The only frost heave in this case is the volume expansion as the pore water converts to ice and  $\dot{h} = \dot{h}_i = 0.09 n V$ .

### 3 Conservation equations

#### 3.1 Water balance at the ice lens

Conservation of mass for the water at the freezing front  $z = X^+$  can be written as

$$\rho_i v_i = \rho_w v_w, \quad (9)$$

where  $v_i = \dot{h}_s$  is the segregated ice growth rate. The water volume velocity  $v_w$  in the unfrozen soil adjacent to the ice lens is given by Darcy's law in the form

$$v_w = \frac{K}{\rho_w g} \left( \frac{\partial p}{\partial z} \right)_{X^+}, \quad (10)$$

where  $K$  is the hydraulic conductivity of the soil at the ice lens surface  $z = X^+$  and  $g$  is the acceleration of gravity. The hydraulic conductivity at the base of the ice lens is much less than that of the unfrozen soil because of the resistance to flow in the premelted films separating the soil particles from the ice [35, 36]. The overburden pressure  $P_{ob}$  reduces the thickness of the premelted films and further decreases the hydraulic conductivity. Here as in previous work [21, 29, 37] it is assumed that  $K$  is given as a function of  $P_{ob}$  by the exponential equation

$$K = K_0 e^{-b P_{ob}}, \quad (11)$$

where  $K_0$  is the zero-overburden hydraulic conductivity at the ice lens and  $b$  is a constant.

##### 3.1.1 Effect of particle trapping on the Darcy flux

With (3a) and (7) Darcy's law (10) can be written in terms of  $k_p$  and  $V$  as

$$v_w = \frac{\rho_i}{\rho_w} (1 - k_p) V = \frac{K}{\rho_w g} \left( \frac{\partial p}{\partial z} \right)_{X^+}. \quad (12)$$

The factor  $(1 - k_p)$  in (12) accounts for the effect of particle trapping on flow to the ice lens. When  $k_p = 0$  equation (12) reduces to Darcy's law for a pure ice lens [10, 29]. When  $k_p = 1$ ,  $\partial p / \partial z = 0$  and there is no flow of water to the ice lens; in this case only *in situ* freezing occurs.

#### 3.2 Heat balance at the ice lens

The boundary condition expressing conservation of energy at the ice lens surface  $z = X(t)$  can be written as

$$\lambda_f \left( \frac{\partial T}{\partial z} \right)_{X^-} - \lambda_u \left( \frac{\partial T}{\partial z} \right)_{X^+} = \rho_i v_i L_f + \rho_i L_f n \dot{X}, \quad (13)$$

where  $\lambda_f$  and  $\lambda_u$  are the thermal conductivities of the frozen and unfrozen soil and  $L_f$  is the latent heat per unit mass of ice [6, 10, 38]. The first term on the right hand side of (13) accounts for the latent heat released by the water flowing from the reservoir as it freezes onto the ice lens, while the second term accounts for the latent heat released as the pore water freezes.

#### 3.3 Hydraulic supercooling and multiple ice lenses

The temperature at the ice lens surface  $z = X$  is given by the Clapeyron equation

$$T = T_{Cl} = T_m - \frac{T_m}{\rho_w L_f} (p_i - p) \quad (z = X), \quad (14)$$

where  $p_i = P_{ob}$  is the pressure on the ice lens and  $p$  is the local fluid pressure in the premelted films separating the ice from the soil particles [15, 35, 39]. The temperature gradient  $G_T = (\partial T / \partial z)_{X^+}$  at the position of the ice lens is not in general equal to the gradient of the Clapeyron temperature  $G_{T_{Cl}} = (\partial T_{Cl} / \partial z)_{X^+}$ . When the temperature gradient is less than the Clapeyron temperature gradient,

$$G_T < G_{T_{Cl}}, \quad (15)$$

the unfrozen soil below the ice lens is hydraulically supercooled [29, 40, 41]. As noted by Palmer [40] and Style *et al.* [41], hydraulic supercooling is a necessary condition for the formation of multiple ice lenses. A linear stability analysis indicates that the supercooled ice lens experiences unstable growth, leading to the formation of a mushy layer composed of a network of vertical ice veins and multiple ice lenses [29, 42–44]. The segregated ice fraction in the mushy layer increases until the hydraulic supercooling has been removed, similar to what occurs during the formation of mushy layers in aqueous solutions and colloidal suspensions [29, 45, 46].

Taking the gradient of the Clapeyron equation (14) gives, assuming  $p_i$  is constant,  $G_{T_{cl}} = (T_m/\rho_w L_f)(\partial p/\partial z)_{X+}$ . Combining this with (12) and inserting into (15) shows that a mushy layer forms when

$$V > \frac{G_T \rho_w L_f K}{T_m \rho_i g (1 - k_p)}. \quad (16)$$

Equation (16) generalizes the condition for hydraulic supercooling in soils obtained previously [29, 41] to allow for particle trapping, which tends to stabilize the ice lens; as  $k_p \rightarrow 1$ , larger freezing rates  $V$  are required to initiate hydraulic supercooling. When  $k_p = 1$  there is no flow to the ice lens ( $\partial p/\partial z = 0$ ); the soil water freezes *in situ* and hydraulic supercooling does not occur. The ice lens can also be stabilized by increasing the temperature gradient  $G_T$  or by increasing the hydraulic conductivity  $K$  at the ice lens surface, for example by modifying the soil chemistry to increase the premelted film thickness [4, 47, 48].

### 3.3.1 Mushy layer model

Similarly to previous work [29], a simple mushy layer model can be used to determine the segregated ice fraction  $\Phi$  and the average segregated ice growth rate  $v_i = \dot{h}_s$  in the mushy layer. Darcy's law at the position of the warmest ice lens can be written as

$$\Phi \frac{\rho_i}{\rho_w} (1 - k_p) V = \frac{K}{\rho_w g} \left( \frac{\partial p}{\partial z} \right). \quad (17)$$

Combining (17) with the Clapeyron equation (14) and the marginal equilibrium condition  $G_T = G_{T_{cl}}$  then gives

$$\Phi = \frac{K \rho_w L_f G_T}{\rho_i g T_m (1 - k_p) V} \quad \text{and} \quad \dot{h}_s = \frac{\rho_w}{\rho_i} v_w = \frac{G_T \rho_w L_f K}{\rho_i T_m g}. \quad (18)$$

Equation (18) indicates that increasing the temperature gradient  $G_T$  or hydraulic conductivity  $K$  will increase the segregated ice fraction  $\Phi$  and the rate of frost heave  $\dot{h}_s$  in the mushy layer regime. The model predicts that during mushy layer growth the segregated ice lens growth rate  $\dot{h}_s$  is independent of both the freezing rate  $V$  and the particle distribution coefficient  $k_p$ , which may explain in part the observations of Beskow described in the Introduction. This is in contrast to the case of a stable ice lens, for which  $\dot{h}_s = (1 - k_p)V$  (equation (7)). It should be noted that the simple model developed here ignores the effects of regelation in the mushy layer, which could become important in systems with a large temperature gradient [49, 50], and could lead to a dependence of  $\dot{h}_s$  on the rate of freezing (Section 4.1).

## 4 The particle distribution coefficient

In order to determine quantitatively the effect of particle trapping on freezing soils, a constitutive equation for the particle distribution coefficient  $k_p$  is required. Expressions for  $k_p(V)$  for spherical particles at an ice surface have been obtained previously by Elliott and Peppin [51] and Sobolev [52, 53]. Here a relatively simple equation of the form

$$k_p = \begin{cases} \frac{V/V_d}{(1 - V^2/V_c^2) + V/V_d}, & (V \leq V_c) \\ 1, & (V > V_c). \end{cases} \quad (19)$$

is used, where  $V_d$  is the freezing speed at which particle trapping first starts to occur in the soil and  $V_c$  is the critical freezing rate above which all particles are trapped [52]. Experiments and

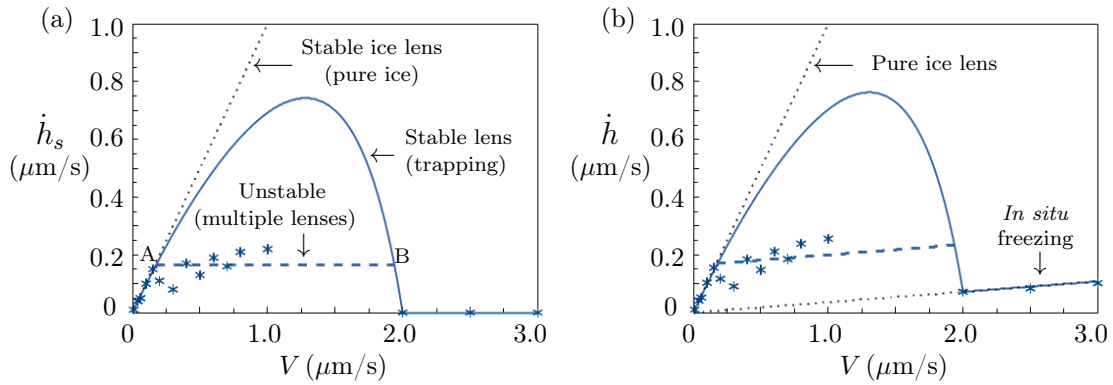


Figure 2: (a) Segregated ice growth rate  $\dot{h}_s$  versus freezing rate  $V$  during unidirectional solidification experiments on a glass powder with average radius  $R = 1.1 \mu\text{m}$  [57]. The dotted (black) curve is the case of a pure ice lens with  $\dot{h}_s = V$ , while the solid curve accounts for particle trapping via equation (20). The horizontal dashed line is the predicted rate of heave at which the ice lens becomes unstable forming a mushy layer. (b) The same data and curves as in (a), with the addition of the *in situ* heave rate  $\dot{h}_i = .09n\dot{X}$ , where  $\dot{X} = V - \dot{h}_s$  is the rate of particle engulfment, giving the total heave rate  $\dot{h} = \dot{h}_s + \dot{h}_i$ .

theory show that  $V_c$  depends in general on the particle radius  $R$ , the temperature gradient  $G_T$ , the overburden pressure  $P_{ob}$ , the pore pressure  $p$  and the surface charge and chemical nature of the soil particles [8, 10, 35, 36, 54–56]. Here it is assumed for simplicity that the critical freezing rate varies inversely with the particle radius  $R$ , such that  $V_c = a/R$ , where  $a$  is a constant [34, 54].

As mentioned in Section 3.1, the present work assumes that the permeability of the unfrozen soil is much larger than the permeability of the premelted films separating the soil from the ice lens, so that  $V_c$  is controlled mainly by film flow [13, 36]. For soils composed of colloidal or nano-sized particles, there is also a dependence of  $V_c$  on the permeability of the soil, as demonstrated by Saint-Michel *et al.* [55] and You *et al.* [56]. Here the focus is on soils with a larger size distribution and increased permeability, for which the pressure drop across the soil is small compared with that across the premelted films [36].

#### 4.1 Steady-state freezing experiments

With (7) and (19), the segregation frost heave rate  $\dot{h}_s$  of a stable planar ice lens with particle trapping can be written as a function of the freezing rate  $V$  as

$$\dot{h}_s = \begin{cases} V \left( 1 - \frac{V/V_d}{(1-V^2/V_c^2)+V/V_d} \right), & (V \leq V_c) \\ 0, & (V > V_c). \end{cases} \quad (20)$$

The solid curve in figure 2 is from equation (20) with  $V_d = 1.0 \mu\text{m/s}$  and  $V_c = 2.0 \mu\text{m/s}$ . The curve represents the predicted rate of frost heave of a stable planar ice lens as the freezing rate  $V$  is increased. At low freezing rates  $V \ll V_c$  equation (20) gives  $\dot{h}_s = V$ , while at higher rates  $\dot{h}_s < V$ . Similar to experiments by Horiguchi [4], Penner [5] and Konrad [6], the segregation heave rate shows a maximum at an intermediate freezing rate before going to zero above the critical rate  $V_c$ .

The horizontal dashed line in figure 2 shows the predicted heave rate at the onset of hydraulic supercooling obtained from equation (16) with  $K = 0.7 \times 10^{-9} \text{m/s}$  and  $G_T = 190^\circ\text{C/m}$  [29, 57]. Once hydraulic supercooling occurs (point A) a mushy layer containing multiple ice lenses forms, and the heave rate no longer obeys (20) but is a constant given by equation (18). At higher  $V$  particle trapping eventually restabilizes the freezing interface (point B) and the heave rate is predicted to again follow equation (20).

The experimental data in figure 2a are from Watanabe [57] using a glass powder medium with average particle radius  $R = 1.1 \mu\text{m}$  and temperature gradient  $G_T = 190^\circ\text{C/m}$ , showing qualitative agreement with the basic features of the model. In particular, Watanabe noted that

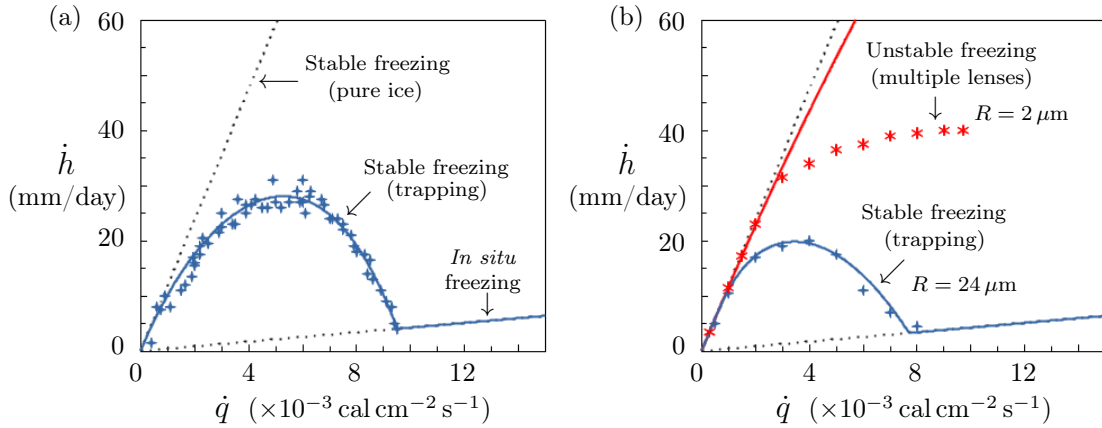


Figure 3: Total frost heave rate  $\dot{h}$  versus the heat extraction rate  $\dot{q}$ . The data in (a) are from Horiguchi [4] using  $R = 20 \mu\text{m}$  zeolite particles, while the data in (b) are from [4] using carborundum particles with  $R = 24 \mu\text{m}$  (crosses) and  $R = 2 \mu\text{m}$  (stars). The curves are from equation (26).

in his experiments the ice lens growth rate  $\dot{h}_s$  was equal to  $V$  up until  $V \approx 0.19 \mu\text{m/s}$ ; then  $\dot{h}_s$  was approximately constant and equal to  $0.24 \mu\text{m/s}$  up until  $V = 2 \mu\text{m/s}$ , above which only *in situ* freezing occurred. The experimental ice lens growth rate varies somewhat in the mushy layer regime between A and B, especially at lower freezing speeds. A potential explanation is regelation, which was neglected in the simple mushy layer model developed in Section 3.3.1. Figure 2b plots the same data as in (a), but showing the total heave rate  $\dot{h} = \dot{h}_s + \dot{h}_i$ , with the *in situ* heave rate calculated as  $\dot{h}_i = 0.09 n \dot{X} = 0.09 n k_p V$ , where  $n = 0.4$  is the porosity.

## 4.2 Transient freezing experiments

While  $V$  is a natural measure of the freezing rate in steady-state unidirectional freezing experiments, during transient step-freezing tests  $V$  is difficult to control. An alternative measure of the freezing rate that has been used is the net rate of heat extraction  $\dot{q}$  [4, 6], defined as

$$\dot{q} = \lambda_f \left( \frac{\partial T}{\partial z} \right)_{X^-} - \lambda_u \left( \frac{\partial T}{\partial z} \right)_{X^+}. \quad (21)$$

Equations (7a), (9), (12) and (13) can be used to write  $\dot{q} = \rho_i L_f V [1 - k_p(1 - n)]$ , showing that  $\dot{q}$  is closely related to  $V$ ; that is,  $\dot{q}/(\rho_i L_f) \rightarrow V$  as  $V \rightarrow 0$  and  $\dot{q}/(\rho_i L_f) \rightarrow nV$  as  $V \rightarrow \infty$ .

Horiguchi [4] performed an experiment in which  $20 \mu\text{m}$  radius zeolite particles were frozen at different heat extraction rates and the total rate of frost heave  $\dot{h}$  was measured as a function of  $\dot{q}$ , with data shown in figure 3. Horiguchi's experiment can be modelled via a similar approach to Section 4.1 by assuming, similar to Arakawa [38], that the heat balance at the freezing front can be separated into two terms, such that

$$(1 - k_p)\dot{q} = \rho_i L_f v_i \quad \text{and} \quad k_p \dot{q} = \rho_i L_f n \dot{X}. \quad (22a,b)$$

That is, a fraction  $(1 - k_p)$  of the heat extraction rate is employed to freeze the excess water volume added to the ice lens from the reservoir, while  $k_p \dot{q}$  is used to freeze the *in situ* pore water. The quantity  $1 - k_p$  in (22) is equivalent to Arakawa's ice segregation efficiency ratio  $E$  [5, 38], defined as

$$E \equiv \sigma L_f / \dot{q} = 1 - k_p, \quad (23)$$

where  $\sigma = \rho_i v_i$  is the rate of mass accumulation of segregated ice. Summing (22a) and (22b) gives the overall heat balance (13). Equations (22), (9) and (3) then give

$$\dot{h}_s = (1 - k_p) \frac{\dot{q}}{\rho_i L_f} \quad \text{and} \quad \dot{h}_i = 0.09 k_p \frac{\dot{q}}{\rho_i L_f}. \quad (24a,b)$$

A constitutive equation for  $k_p(\dot{q})$  in a form similar to equation (19) is

$$k_p = \begin{cases} \frac{\dot{q}/\dot{q}_d}{(1-\dot{q}^2/\dot{q}_c^2)+\dot{q}/\dot{q}_d}, & (\dot{q} \leq \dot{q}_c) \\ 1, & (\dot{q} > \dot{q}_c) \end{cases} \quad (25)$$

where  $\dot{q}_d$  is the heat extraction rate at which particle trapping first starts to occur and  $\dot{q}_c$  is the critical rate above which all particles are trapped. The total frost heave rate  $\dot{h} = \dot{h}_s + \dot{h}_i$  can then be written as

$$\dot{h} = \begin{cases} \frac{\dot{q}}{\rho_i L_f} \left( 1 - \frac{\dot{q}/\dot{q}_d}{(1-\dot{q}^2/\dot{q}_c^2)+\dot{q}/\dot{q}_d} \right) + \dot{h}_i, & (\dot{q} \leq \dot{q}_c) \\ \dot{h}_i, & (\dot{q} > \dot{q}_c), \end{cases} \quad (26)$$

where  $\dot{h}_i = 0.09 k_p \dot{q} / (\rho_i L_f)$ .

Equation (26) is plotted on figure 3a as the solid curve using the best-fit values  $\dot{q}_d = 5.7 \times 10^{-3} \text{ cal cm}^{-2} \text{ s}^{-1}$  and  $\dot{q}_c = 9.5 \times 10^{-3} \text{ cal cm}^{-2} \text{ s}^{-1}$ , and porosity  $n = 0.4$ , giving a good match to Horiguchi's data (crosses). Similarly to figure 2, at low freezing rates  $\dot{h} = \dot{q}/\rho_i L_f = V$ , corresponding to the growth of a pure ice lens (primary frost heave), while at high freezing rates  $\dot{h} = \dot{h}_i$  (*in situ* frost heave). In contrast to figure 2, however, Horiguchi's data appears to follow the trapping curve (26) at all freezing rates. This suggests that the primary ice lens remained stable in his system, and a mushy layer composed of multiple lenses did not form. Horiguchi used a relatively large particle size ( $R = 20 \mu\text{m}$ ) so that particle trapping may have stabilized the interface at all  $\dot{q}$  and hydraulic supercooling did not occur.

This possibility is supported by other experiments in which Horiguchi varied the average particle size of the soil [4]. Figure 3b shows data obtained using carborundum particles with radius  $R = 24 \mu\text{m}$  (crosses) and  $R = 2 \mu\text{m}$  (stars). The solid blue curve for the larger particles is from equation (26) with best-fit values  $\dot{q}_d = 3.5 \times 10^{-3} \text{ cal cm}^{-2} \text{ s}^{-1}$  and  $\dot{q}_c = 7.3 \times 10^{-3} \text{ cal cm}^{-2} \text{ s}^{-1}$ ; the red curve for the smaller particles assumes an  $R^{-1}$  dependence giving values for  $\dot{q}_c$  and  $\dot{q}_d$  that are 12 times larger. For the larger particles the results are similar to figure 3a, with the data following the trapping curve at all  $\dot{q}$ . For the smaller particles, however, the data flattens at a critical heat flux  $\dot{q} \approx 2 \times 10^{-3} \text{ cal cm}^{-2} \text{ s}^{-1}$  and the heave rate becomes approximately independent of the freezing rate, similar to the glass powder results in figure 2. Using  $\rho_i = 0.91 \text{ g cm}^{-3}$  and  $L_f = 80 \text{ cal/g}$  the critical heat flux corresponds to a freezing rate of  $V \approx \dot{q}/(\rho_i L_f) = 0.27 \mu\text{m/s}$ , which is close to the value  $0.19 \mu\text{m/s}$  obtained by Watanabe [57] for  $R = 1.1 \mu\text{m}$  silica particles (Section 4.1). This suggests that hydraulic supercooling leading to a mushy layer with multiple ice lenses may have occurred in Horiguchi's experiment with the  $2 \mu\text{m}$  particles, while particle trapping stabilized the primary ice lens in the system with  $24 \mu\text{m}$  particles.

## 5 Kinetic segregation potential

As mentioned in the Introduction, Konrad and Morgenstern [13] defined the segregation potential  $SP$  as the water flow rate  $v_w$  to the warmest ice lens divided by the temperature gradient  $G_T$  at the onset of the final stable ice lens in a transient frost heave experiment. On the basis of experimental data they obtained the correlation

$$SP = SP_0 e^{-b P_{ob}}, \quad (27)$$

where  $SP_0$  and  $b$  are constants.

Assuming that the onset of the final ice lens corresponds to a state of marginal stability of the ice interface, a linear stability analysis leads to the expression (for non-saline soils) [29]

$$SP = \frac{L_f K}{T_m g}. \quad (28)$$

A similar equation for  $SP$  was obtained earlier by Horiguchi [58]. Comparison of (28), (27) and (11) gives  $K_0 = SP_0 T_m g / L_f$ . Equations (28) and (27) imply that  $SP$  is independent of the freezing rate; however, experiments by Konrad and Morgenstern [17, 27], Svec [26] and Kim [59] show that during the early stages of transient frost heave experiments the measured segregation potential  $SP = v_w / G_T$  depends on the freezing rate and can be much smaller than predicted by (27) or (28).

Here, motivated by equation (7), the dependence of  $SP$  on the freezing rate is accounted for by using a kinetic segregation potential of the form

$$SP_{kin} = (SP)E = \frac{L_f K}{T_m g} (1 - k_p), \quad (29)$$

where  $E = 1 - k_p$  is Arakawa's ice segregation efficiency ratio [38] described in Section 4.2. Equation (29) with (19) or (25) for  $k_p$  shows that  $SP_{kin} \rightarrow 0$  during the early rapid freezing stage of a transient frost heave experiment, while  $SP_{kin} \rightarrow SP$  at later stages involving slower freezing rates. In the next section equation (29) is used to model the frost heave rate during the early stages of a field frost heave experiment and above a buried natural gas pipeline.

## 6 Field frost heave experiments

As noted by Konrad and Morgenstern [16] and Nixon [18], robust estimates of the temperature profile and depth of freezing in many field situations are known either from experimental data or from models such as the modified Berggren equation [60]. Assuming the depth of freezing  $X(t)$  is known, along with the temperature gradient  $G_T(t)$  at the freezing front, Konrad and Morgenstern [16] suggest that the total frost heave rate  $h(t)$  can be approximated by the equation

$$h(t) = 1.09 \int_0^t v_w dt + 0.09 n X(t), \quad (30)$$

where

$$v_w = SP G_T \quad (31)$$

is the water intake rate. The first term on the right-hand side of (30) accounts for the segregated ice lens growth while the second term accounts for the 9% volume expansion as the pore water freezes. Konrad and Morgenstern [16] suggest that in many field situations  $X(t)$  and  $G_T(t)$  obey power laws of the form  $at^b$ , where  $a$  and  $b$  are constants.

Equations (30) and (31) have been used successfully to model frost heave by several researchers, including Konrad and Morgenstern [21], Konrad and Shen [22], Nixon [18], Carlson and Nixon [20], Kim *et al.* [61] and Yu *et al.* [62]. However, as acknowledged by Konrad and Morgenstern [16] and noted subsequently by Segoo *et al.* [25] and Nixon [30, 63], the correlation (27) breaks down at high freezing rates, when the water intake rate  $v_w$  approaches zero (or can even be negative with water expulsion).

Here a similar approach to Konrad and Morgenstern [16] and Nixon [18] is taken, but with a water flux of the form

$$v_w = SP_{kin} G_T = SP G_T (1 - k_p). \quad (32)$$

Given that neither the total freezing rate  $V$  nor the heat extraction rate  $\dot{q}$  are typically known in field situations, it is proposed to use for  $k_p$  a simpler constitutive equation of the form

$$k_p = \frac{\dot{X}/V_d}{1 + \dot{X}/V_d}, \quad (33)$$

where  $\dot{X} = dX/dt$  is the rate at which the freezing front moves into the soil and  $V_d$  is the freezing rate at which particle trapping first starts to occur in the soil. Equation (33) has a simpler form than (19) and (25) while still capturing the expectation that  $k_p \rightarrow 1$  during the early rapid-freezing stages of soil freezing, while  $k_p \rightarrow 0$  at later slower stages.

### 6.1 Circular plate experiment

As a test of equations (30)–(33), in this section they are applied to field frost heave data obtained by Nixon *et al.* [18, 64], shown on figures 4 and 5. They conducted frost heave experiments on a soil (Calgary silt, porosity  $n = 0.38$  [21]) below a 0.76 m diameter circular cold plate held at the constant temperature  $T_c = -4^\circ\text{C}$ . Figure 4 shows measured data for the depth of freezing  $X(t)$

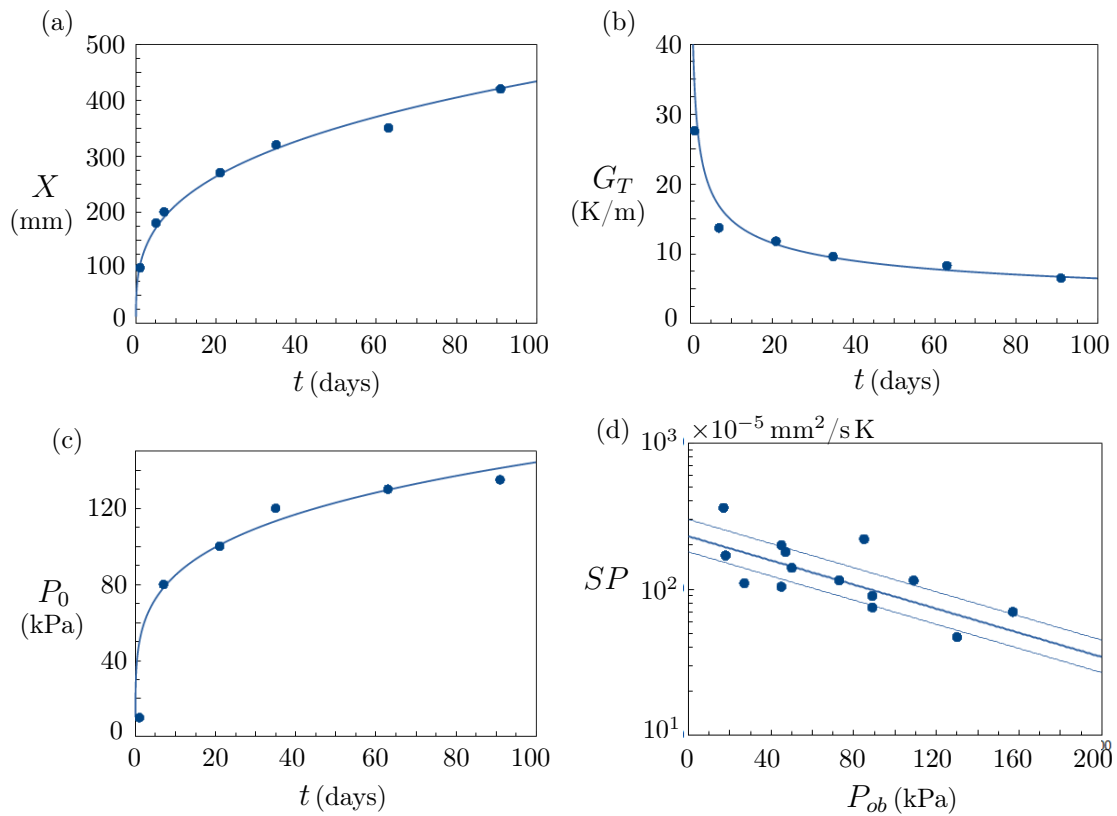


Figure 4: (a) Data for the position of the  $0^\circ\text{C}$  isotherm  $X(t)$  in soil (Calgary silt) below a 0.76 m diameter plate cooled to  $-4^\circ\text{C}$ . (b) Temperature gradient measurements at the position of the freezing front  $X(t)$ . (c) Soil pressure  $P_0(t)$  measured at the level of the cooling plate. The data in (a-c) were obtained by Nixon *et al.* [18, 64], while the curves are from equations (34). (d) Segregation potential data for Calgary silt obtained by Konrad and Morgenstern [21].

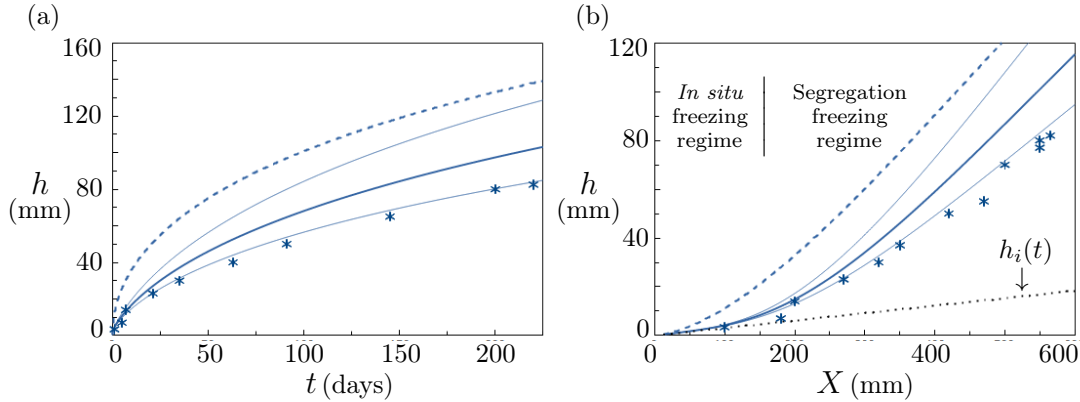


Figure 5: (a) Total heave  $h(t)$  data (stars) measured at the surface of a soil cooled by a 0.76 m diameter copper plate held at  $-4^\circ\text{C}$  [18]. The dashed curve is the predicted heave using the segregation potential  $SP$  model given by (27) and (36). The solid curve is the predicted heave using the kinetic segregation potential  $SP_{kin} = SP(1 - k_p)$ , with  $k_p$  given by (33). The thin solid curves use the lower and upper bound segregation potential curves from figure 4d:  $SP_0 = 180 \times 10^{-5} \text{mm}^2/(\text{C s})$  (lower bound) and  $SP_0 = 300 \times 10^{-5} \text{mm}^2/(\text{C s})$  (upper bound) [21]. (b) Plot of total heave  $h(t)$  versus freezing depth  $X(t)$ , illustrating an *in situ* freezing regime at early times, in which the measured heave rate is very close to the predicted *in situ* heave  $h_i(t)$  (black dotted line). A segregation freezing regime involving multiple segregated ice lenses occurs at later times [64]. The blue curves are the same as in (a) but plotted versus  $X(t)$ .

below the plate, the temperature gradient  $G_T(t)$  at the freezing front and the soil pressure  $P_0(t)$  at the level of the plate, along with the power law correlations

$$X = 104 t^{0.31} \text{ (mm)}, \quad G_T = 0.034 t^{-0.36} \text{ (}^\circ\text{C/mm)} \quad \text{and} \quad P_0 = 47 t^{0.23} \text{ (kPa)}, \quad (34a,b,c)$$

which provide good fits to the data up to  $t = 100$  days. Given the depth of freezing  $X(t)$  and the approximate frozen soil density  $\rho \approx 1 \text{ g/cm}^3$  [20], the total overburden pressure at the freezing front can be estimated as

$$P_{ob} = P_0 + \rho g X \approx P_0(t) + 0.01 X(t), \quad (35)$$

with  $P_0(t)$  in kPa and  $X(t)$  in mm [20].

For the Calgary silt used by Nixon *et al.* [64], Konrad and Morgenstern [21] obtained data for the segregation potential  $SP$ , shown in figure 4d along with the correlation (27) with best-fit parameters

$$SP_0 = 230 \times 10^{-5} \text{mm}^2/(\text{C s}) \quad \text{and} \quad b = 0.0095 \text{ kPa}^{-1}. \quad (36)$$

Figure 4d also shows the lower and upper bounds on  $SP$  suggested by Konrad and Morgenstern [21], with  $SP_0 = 180 \times 10^{-5} \text{mm}^2/(\text{C s})$  (lower bound) and  $SP_0 = 300 \times 10^{-5} \text{mm}^2/(\text{C s})$  (upper bound). With (34)–(36) and either (31) or (32) for  $v_w$ , equation (30) can be integrated numerically, giving the results shown in figure 5a. The dashed curve is the predicted total heave  $h(t)$  of the soil using the segregation potential model (31). As noted by Konrad and Morgenstern [27], the model gives an accurate prediction of the heave rate (slope of the curve) at later times, but tends to overpredict  $h(t)$  at early times when the freezing rate is high. Accounting for particle trapping via equation (32) (solid curves) leads to a closer match to the early time data. Here a value  $V_d = 9 \text{ mm/day} \approx 0.1 \mu\text{m/s}$  for the trapping speed has been used, which is close to the critical trapping speed measured by Cisse and Bolling [34] for glass spheres with radius  $100 \mu\text{m}$ . This value corresponds to the largest 5 – 10% of particles in Calgary silt [64], supporting the interpretation of  $V_d$  as the freezing speed at which particle trapping starts to become significant within the soil.

Figure 5b shows the same data and curves plotted as the frost heave  $h(t)$  versus the freezing depth  $X(t)$ . In this form two distinct freezing regimes can be discerned – an *in situ* regime at early times during which  $h = h_i$ , and a segregation regime at later times when  $h = h_i + h_s$  [64]. The lower dotted line shows the calculated *in situ* heave  $h_i(t) = 0.09 n X(t)$ , in good agreement with the early time data.

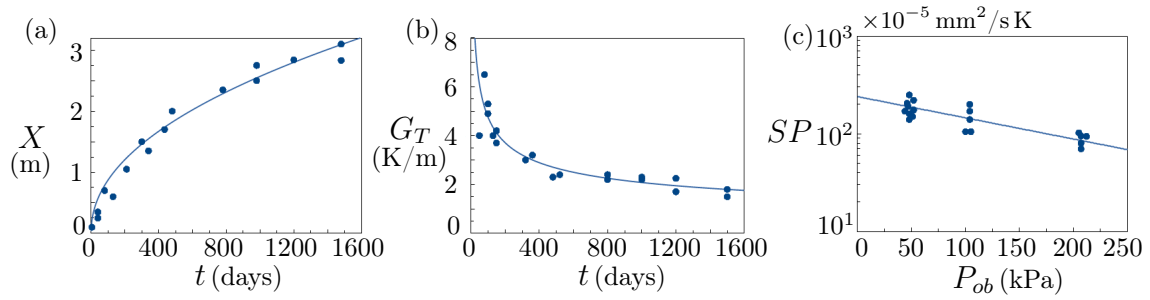


Figure 6: (a) Position of the 0 °C isotherm  $X(t)$  in soil below a buried natural gas pipeline cooled to -8.5 °C [64]. (b) Temperature gradient measurements at the position of the freezing front  $X(t)$  [64]. (c) Segregation potential data for Calgary silt obtained by Carlson and Nixon [20].

## 6.2 Buried pipeline experiment

As a further test of the model, figures 6 and 7 show frost heave data obtained by Carlson *et al.* [65] below a buried pipeline held at  $T_c = -8.5$  °C. Figure 6 shows data for the depth of freezing  $X(t)$  and temperature gradient  $G_T(t)$  at the freezing front, which are approximated by power law expressions of the form

$$X = 100t^{0.47} \text{ (mm)} \quad \text{and} \quad G_T = 0.025t^{-0.36} \text{ (°C/mm)}, \quad (37a,b)$$

with  $t$  in days. In this experiment a similar soil (Calgary silt) was used, but at a lower depth. Segregation potential  $SP$  data from Carlson and Nixon [20] is shown in figure 6c, giving the best-fit parameters

$$SP_0 = 240 \times 10^{-5} \text{ mm}^2/(\text{°C s}) \quad \text{and} \quad b = 0.05 \text{ kPa}^{-1}. \quad (38)$$

The initial overburden pressure at the level of the pipe was estimated by Carlson and Nixon [20] as 48 kPa, and at  $t = 420$  days a 30 kPa berm was added to the surface, giving the total overburden pressure at the freezing front  $X(t)$  as

$$P_{ob} = \begin{cases} 48 + 0.01 X(t), & 0 < t < 420 \text{ days} \\ 78 + 0.01 X(t), & t \geq 420 \text{ days,} \end{cases} \quad (39)$$

with  $X(t)$  in mm and  $P_{ob}$  in kPa [20].

With (37)–(39) equation (30) can be integrated to determine  $h(t)$ , as shown by the blue curves in figure 7. Again the  $SP$  model (dashed curve) tends to overestimate the rate of frost heave at early times. The model with particle trapping gives a closer match to the early time data, using the same value for the trapping speed  $V_d = 9$  mm/day as in Section 6.1.

## 6.3 Saline soils

Many soils contain a significant salt content [66], in which case the segregation potential can be influenced by the salt diffusivity  $D$  as well as the hydraulic conductivity  $K$  [17, 29]. In saline soils the segregation potential can be written in the form

$$SP = \left( \frac{T_m g}{L_f K} + \frac{m c_0 (1 - k_s)}{D k_s} \right)^{-1}, \quad (40)$$

where  $m$  is the slope of the solute freezing temperature curve (for NaCl  $m = 0.065$  °C L/g),  $c_0$  is the solute concentration of the pore fluid,  $D \approx D_0 e^{-b P_{OB}}$  is the solute diffusivity in the premelted films and  $k_s$  is the solute distribution coefficient at the ice lens [29].

With particle trapping the kinetic segregation potential in saline soils can be written as

$$SP_{kin} = (SP)E = \frac{1 - k_p}{\left( \frac{T_m g}{L_f K} + \frac{m c_\infty (1 - k_s)}{D k_s} \right)}. \quad (41)$$

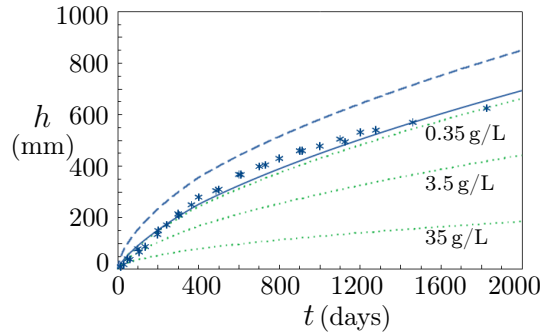


Figure 7: Total heave  $h(t)$  measured in the buried pipeline experiment (deep burial section) [18]. The dashed curve is the predicted heave using the segregation potential  $SP$  given by (27). The solid curve uses the kinetic segregation potential  $SP_{kin} = SP(1 - k_p)$ , with  $k_p$  given by (33). The dotted green curves show the predicted effect of increasing the salinity  $c_0$  of the soil, with  $SP_{kin}$  given by equation (41).

Using (41) with (30), (32) and (33) allows the effect of soil salinity on frost heave in field situations to be predicted. The green dotted curves in figure 7 show the effect of soil salinity on the rate of frost heave in the buried pipeline experiment for the case  $k_s = 0.4$ ,  $D_0 = 10^{-9} \text{ m}^2/\text{s}$  and various  $c_0$ , with other parameters the same as in Section 6.2. A moderate salt concentration of 3.5 g/L significantly decreases the rate of frost heave, in qualitative agreement with the observations of Sheeran and Young [67, 68], Chamberlain [42], Velsovskij *et al.* [69] and Liu *et al.* [70].

In equation (41) the salt distribution coefficient  $k_s$  at the ice lens surface has been treated for simplicity as an averaged constant; more generally  $k_s$  also depends on the freezing rate [71–73]. Qualitatively similar results can be obtained by replacing  $k_s$  in equation (41) with a kinetic salt distribution coefficient of the form  $k_v = k_s/[k_s + (1 - k_s)e^{-\alpha\dot{X}}]$  [72]. This equation requires knowledge of the additional parameter  $\alpha$ . For saline sands Baker and Osterkamp [72] obtained  $k_s = 0.34$  and  $\alpha = 0.076 \text{ days/mm}$ ; experiments by Konrad and McCammon [73] suggest that  $k_s$  and  $\alpha$  are of similar magnitude for silty clay soils.

## 7 Discussion

In this work effects such as regelation within the mushy layer and consolidation have been neglected. These effects may be important in some systems, as discussed briefly in Section 4.1. However, in field situations involving relatively small temperature gradients and high freezing rates, in soils with a broad size distribution, regelation will be less of an issue (at least at relatively short time scales), and it is anticipated that particle trapping will have a more significant effect on the segregation potential  $SP$ . Developing a model of the effects of regelation and consolidation on  $SP$  is left to future work. The present model also assumes that the depth of freezing  $X(t)$  and temperature gradient  $G_T(t)$  are known, either experimentally or from alternative models. A complete model should predict these quantities, along with the average segregated ice fraction  $\Phi$  in the mushy region. A preliminary approach to modelling mushy layers in colloidal suspensions, including the effects of regelation, has been obtained recently [50]; it may be possible to extend this work to the present system, yielding a partial differential equation for the ice fraction  $\Phi(z, t)$ , and this will be explored in future work.

## 8 Conclusions

A model of frost heaving soils has been developed that takes account of particle trapping effects. An expression for the particle distribution coefficient at the ice lens surface has been obtained, and compared with experimental data on a range of model soils. Particle trapping tends to stabilize the ice lens and reduce the amount of frost heave. Based on these results a new kinetic expression for

the segregation potential has been developed that accounts for particle trapping and depends on the freezing rate. The new expression is the product of Konrad and Morgenstern's [13] segregation potential  $SP$  and Arakawa's [38] ice segregation efficiency ratio  $E$ . This leads to a kinetic version of Konrad and Morgenstern's field frost heave model that simulates the *in situ* freezing that occurs at early times in step freezing tests. The model predictions have been compared to frost heave data obtained on soil below a cooled circular plate and below a chilled natural gas pipeline. For field situations in which the depth of freezing and temperature gradient at the freezing front are known from independent measurements or models, the present method provides a simple approach to predict the total frost heave rate as a function of the freezing rate and overburden pressure in both saline and non-saline soils.

## Acknowledgements

This work was made possible by the love and support of Jesus, Lord of heaven and earth and Saviour of all who believe. *Believe on the Lord Jesus Christ and thou shalt be saved, and thy house.* Acts 16:31. *The heaven, even the heavens, are the LORD'S: but the earth hath He given to the children of men* Psalm 115:16.

## References

- [1] Peter J. Williams and Michael W. Smith. *The Frozen Earth: Fundamentals of Geocryology*. Cambridge University Press, UK, 1989.
  - [2] S. Taber. Frost heaving. *J. Geol.*, **37**, 428–461, 1929.
  - [3] G. Beskow. *The Swedish Geological Society, C, no. 375, Year Book no. 3*. Technological Institute, Northwestern University, 1935. Reprinted in *Historical Perspectives in Frost Heave Research* (P. B. Black and M. J. Hardenberg, eds.) CRREL Special Report No. 91-23, pp 37–157, 1991.
  - [4] K. Horiguchi. Effect of the rate of heat removal on the rate of frost heaving. *Engineering Geology*, **13**, 63–71, 1979.
  - [5] E. Penner. Influence of freezing rate on frost heaving. *Highway Res. Rep.*, **393**, 56–64, 1972.
  - [6] J. M. Konrad. Procedure for determining the segregation potential of freezing soils. *Geotechnical Testing Journal*, **10**, 51–58, 1987.
  - [7] A. E. Corte. The frost behavior of soils. Field and laboratory data for a new concept. 1, Vertical sorting. *CRREL Res. Rep.*, **85**, 9–34, 1961.
  - [8] A. E. Corte. Vertical migration of particles in front of a moving freezing plane. *Journal of Geophysical Research*, **67**, 1085–1090, 1962.
  - [9] A. E. Corte. Particle sorting by repeated freezing and thawing. *Science*, **142**, 499–501, 1963.
  - [10] D. R. Uhlmann, B. Chalmers, and K. A. Jackson. Particle sorting and stone migration due to frost heave. *Science*, **152**, 545–546, 1966.
  - [11] Julia Branson. Preferential incorporation of coarse sediment during needle ice growth: A preliminary analysis. In *Proceedings of the 7th International Conference on Permafrost*, pages 75–82, Yellowknife, Canada, 1998.
  - [12] Norikazu Matsuoka, Miwa Abe, and Manabu Ijiri. Differential frost heave and sorted patterned ground: field measurements and a laboratory experiment. *Geomorphology*, **52**, 73–85, 2003.
  - [13] J. M. Konrad and N. R. Morgenstern. The segregation potential of a freezing soil. *Canadian Geotechnical Journal*, **18**, 482–491, 1981.
-

- [14] K. Watanabe and M. Mizoguchi. Ice configuration near a growing ice lens in a freezing porous medium consisting of micro glass particles. *J. Cryst. Growth*, **213**, 135–140, 2000.
- [15] S. S. L. Peppin and R. W. Style. The physics of frost heave and ice-lens growth. *Vad. Zone J.*, **12**, 1–12, 2013.
- [16] J. M. Konrad and N. R. Morgenstern. Effects of applied pressure on freezing soils. *Canadian Geotechnical Journal*, **19**, 494–505, 1982.
- [17] J.-M. Konrad. Segregation potential - pressure - salinity relationships near thermal steady state for a clayey silt. *Canadian Geotechnical Journal*, **27**, 203–215, 1990.
- [18] J. F. Nixon. Field frost heave predictions using the segregation potential concept. *Canadian Geotechnical Journal*, **19**, 526–529, 1982.
- [19] M. Fukuda and S. Kinoshita. Field frost heave prediction related to ice segregation processes during soil freezing. *Annals of Glaciology*, **6**, 87–91, 1985.
- [20] L. E. Carlson and J. F. (Derick) Nixon. Subsoil investigation of ice lensing at the Calgary, Canada, frost heave test facility. *Canadian Geotechnical Journal*, **25**, 307–319, 1988.
- [21] J.-M. Konrad and N. R. Morgenstern. Frost heave prediction of chilled pipelines buried in unfrozen soils. *Canadian Geotechnical Journal*, **21**, 100–115, 1984.
- [22] J.-M. Konrad and M. Shen. 2-D frost action modeling using the segregation potential of soils. *Cold Regions Science and Technology*, **24**, 263–278, 1996.
- [23] J.-M. Konrad. Prediction of freezing-induced movements for an underground construction project in Japan. *Canadian Geotechnical Journal*, **39**, 1231–1242, 2002.
- [24] Jie Zhou, Wenqiang Zhao, and Yiqun Tang. Practical prediction method on frost heave of soft clay in artificial ground freezing with field experiment. *Tunnelling and Underground Space Technology*, **107**, 103647, 2021.
- [25] W. van Gassen and D.C. Segó. Problems with the segregation potential theory. *Cold Regions Science and Technology*, **17**, 95–97, 1989.
- [26] O. J. Svec. A new concept of frost-heave characteristics of soils. *Cold Regions Science and Technology*, **16**, 271–279, 1989.
- [27] J. M. Konrad and N. R. Morgenstern. Prediction of frost heave in the laboratory during transient freezing. *Canadian Geotechnical Journal*, **19**, 250–259, 1982.
- [28] J.-M. Konrad and J. T. C. Seto. Frost heave characteristics of undisturbed sensitive Champlain sea clay. *Canadian Geotechnical Journal*, **31**, 285–298, 1994.
- [29] S. S. L. Peppin. Stability of ice lenses in saline soils. *Journal of Fluid Mechanics*, **886**, A16, 2020.
- [30] J. F. (Derick) Nixon. Discrete ice lens theory for frost heave in soils. *Canadian Geotechnical Journal*, **28**, 843–859, 1991.
- [31] Edward C McRoberts and Norbert R. Morgenstern. Pore water expulsion during freezing. *Canadian Geotechnical Journal*, **12**, 130–141, 1975.
- [32] E. Penner and T. Ueda. The dependence of frost heaving on load application - preliminary results. In *Proc. Int. Symp. on Frost Action in Soils*, pages 92–101, Lulea, Sweden, 1977.
- [33] D. R. Uhlmann, B. Chalmers, and K. A. Jackson. Interaction between particles and a solid/liquid interface. *J. Appl. Phys.*, **35**, 2986–2992, 1964.
- [34] J. Cissé and G. G. Bolling. A study of the trapping and rejection of insoluble particles during the freezing of water. *Journal of Crystal Growth*, **10**, 67–76, 1971.
-

- [35] M. G. Worster and J. S. Wettlaufer. *The Fluid Mechanics of Premelted Liquid Films*, pages 339–351. Fluid Dynamics at Interfaces. Cambridge University Press, Cambridge, UK, 1999.
- [36] R. W. Style and S. S. L. Peppin. The kinetics of ice-lens growth in porous media. *J. Fluid Mech.*, **692**, 482–498, 2012.
- [37] P. Black. Three functions that model empirically measured unfrozen water content and predict relative hydraulic conductivity. *CRREL Tech. Rep.*, **90-5**, 1–7, 1990.
- [38] Kiyoshi Arakawa. Theoretical studies of ice segregation in soil. *Journal of Glaciology*, **6**, 255–260, 1966.
- [39] P. Black. Applications of the Clapeyron equation to water and ice in porous media. *CRREL Tech. Rep.*, **95-6**, 1–7, 1995.
- [40] Andrew C. Palmer. Ice lensing, thermal diffusion and water migration in freezing soil. *Journal of Glaciology*, **6**, 681–694, 1967.
- [41] R. W. Style, S. S. L. Peppin, A. C. F. Cocks, and J. S. Wettlaufer. Ice lens formation and geometrical supercooling in soils and other colloidal materials. *Phys. Rev. E*, **84**, 041402, 2011.
- [42] E. J. Chamberlain. Frost heave of saline soils. In *Proceedings of the 4th International Conference on Permafrost*, pages 121–126, Fairbanks, Alaska, 1983.
- [43] L. U. Arenson, D. Xia, D. C. Sego, and K. W. Biggar. Change in ice lens formation for saline and non-saline Devon silt as a function of temperature and pressure. In *Cold Regions Engineering 2006: Current Practices in Cold Regions Engineering*, pages 1–11, 2006.
- [44] Hao Zheng, Yuutarou Sasaki, and Shunji Kanie. Image processing method for observing ice lenses produced by the frost heave process. *Cold Regions Science and Technology*, **171**, 102977, 2020.
- [45] M. G. Worster. Solidification of an alloy from a cooled boundary. *Journal of Fluid Mechanics*, **167**, 481–501, 1986.
- [46] M. G. Worster, S. S. L. Peppin, and J. S. Wettlaufer. Colloidal mushy layers. *Journal of Fluid Mechanics*, **914**, A28, 2021.
- [47] E. S. Thomson, H. Hansen-Goos, J. S. Wettlaufer, and L. A. Wilen. Grain boundary melting in ice. *The Journal of Chemical Physics*, **138**, 124707, 2013.
- [48] Margaret M. Darrow and Ross M. Lieblappen. Visualizing cation treatment effects on frozen clay soils through  $\mu$ CT scanning. *Cold Regions Science and Technology*, **175**, 103085, 2020.
- [49] Siyu Chen, Julia M. H. Schollick, Roel P. A. Dullens, and Dirk G. A. L. Aarts. Thermal regelation of a single particle, arXiv:2006.15625, 2020.
- [50] Jiaxue You, Zhijun Wang, and M. Grae Worster. Thermal regelation of single particles and particle clusters in ice. *Soft Matter*, **17**, 1779–1787, 2021.
- [51] J. A. W. Elliott and S. S. L. Peppin. Particle trapping and banding in rapid colloidal solidification. *Phys. Rev. Lett.*, **107**, 168301, 2011.
- [52] S.L. Sobolev. Local non-equilibrium diffusion model for solute trapping during rapid solidification. *Acta Materialia*, **60**, 2711–2718, 2012.
- [53] S.L. Sobolev. Rapid colloidal solidifications under local nonequilibrium diffusion conditions. *Physics Letters A*, **376**, 3563–3566, 2012.
- [54] A. W. Rempel and M. G. Worster. The interaction between a particle and an advancing solidification front. *J. Cryst. Growth*, **205**, 427–440, 1999.
-

- [55] Brice Saint-Michel, Marc Georgelin, Sylvain Deville, and Alain Pocheau. Interaction of multiple particles with a solidification front: From compacted particle layer to particle trapping. *Langmuir*, **33**, 5617–5627, 2017.
- [56] J. You, Z. Wang, and M. G. Worster. Controls on microstructural features during solidification of colloidal suspensions. *Acta Materialia*, **157**, 288–297, 2018.
- [57] Kunio Watanabe. Relationship between growth rate and supercooling in the formation of ice lenses in a glass powder. *Journal of Crystal Growth*, **237-239**, 2194–2198, 2002.
- [58] Kaoru Horiguchi. An osmotic model for soil freezing. *Cold Regions Science and Technology*, **14**, 13–22, 1987.
- [59] K. Kim. *Multi-Dimensional Frost Heave Modeling With SP Porosity Growth Function*. PhD thesis, University of Alaska, Fairbanks, Alaska, 2011.
- [60] Barret L. Kurylyk and Masaki Hayashi. Improved Stefan equation correction factors to accommodate sensible heat storage during soil freezing or thawing. *Permafrost and Periglacial Processes*, **27**, 189–203, 2016.
- [61] Kouli Kim, Wei Zhou, and Scott L. Huang. Frost heave predictions of buried chilled gas pipelines with the effect of permafrost. *Cold Regions Science and Technology*, **53**, 382–396, 2008.
- [62] Fan Yu, Peijun Guo, Yuanming Lai, and Dieter Stolle. Frost heave and thaw consolidation modelling. Part 1: A water flux function for frost heaving. *Canadian Geotechnical Journal*, **57**, 1581–1594, 2020.
- [63] J. F. Nixon, K. A. Sortland, and D. A. James. Geotechnical aspects of northern gas pipeline design. In *Permafrost Canada: Proceedings of the Fifth Canadian Permafrost Conference*, pages 299–307, 1990.
- [64] J. F. Nixon, J. R. Ellwood, and W. A. Slusarchuk. *In situ* frost heave testing using cold plates. In *Proceedings of the 4th Canadian Permafrost Conference*, volume 1, pages 466–474, 1982.
- [65] L. E. Carlson, J. R. Ellwood, J. F. Nixon, and W. A. Slusarchuk. Field test results of operating a chilled, buried pipeline in unfrozen ground. In *Proceedings of the 4th Canadian Permafrost Conference*, volume 1, pages 475–480, 1982.
- [66] E.G. Hivon and D.C. Segó. Distribution of saline permafrost in the Northwest Territories, Canada. *Canadian Geotechnical Journal*, **30**, 506–514, 1993.
- [67] D. E. Sheeran and R. N. Yong. Water and salt redistribution in freezing soils. In *Proceedings, Conference on Soil-Water Problems in Cold Regions*, pages 58–69, Calgary, Alberta, 1979.
- [68] K. Henry. Chemical aspects of soil freezing. *CRREL Res. Rep.*, **88-17**, 1–8, 1988.
- [69] A. Y. Velsovskij, V. A. Shorin, and T. R. Akhmetov. Study of the influence of chemical anti-icing materials on frost heaving of the roadbed soils. In *E3S Web of Conferences*, volume 220 of *E3S Web of Conferences*, page 01064, 2020.
- [70] Jianpeng Liu, Ping Yang, and Zhaohui Yang. Water and salt migration mechanisms of saturated chloride clay during freeze-thaw in an open system. *Cold Regions Science and Technology*, **186**, 103277, 2021.
- [71] G. F. N. Cox and W. F. Weeks. Brine drainage and initial salt entrapment in sodium chloride ice. *CRREL Res. Rep.*, **345**, 1–85, 1975.
- [72] G. C. Baker and T. E. Osterkamp. Salt redistribution during freezing of saline sand columns at constant rates. *Water Resources Research*, **25**, 1825–1831, 1989.
- [73] J.-M. Konrad and A. W. McCammon. Solute partitioning in freezing soils. *Canadian Geotechnical Journal*, **27**, 726–736, 1990.
-